

STANDING CONTACT FATIGUE WITH LINE LOADING

Johan Dahlberg and Bo Alfredsson
Department of Solid Mechanics at KTH,
100 44 Stockholm, Sweden
johand@hallf.kth.se

Abstract

In order to simulate sub-surface cracking due to contact loads a purified contact fatigue experiment was adopted to a two-dimensional cylindrical contact. Contact fatigue cracks developed primarily below the surface, but for substantially increased loads and for longer test runs, surface cracks did also develop. The order in which the cracks appeared was established by strain measurements and crack observations at test termination. The non-zero surface strain response was verified analytically and numerically.

Introduction

Damage due to contact fatigue can be divided into two major groups; surface initiated and sub-surface initiated spalling. In both cases of crack initiation, the crack undermines the surrounding material through propagation and finally it causes a surface damage as the undermined piece of material is lost to the contact surface. The surface damage is often denoted surface spall or sub-surface spall depending on the initiation site. So far no generally accepted mechanism exists for any of these two spalling groups. Gears, bearings and cams with followers are typical contact applications where this type of problems may arise. The current work focused on an explaining mechanism for sub-surface initiated contact fatigue cracks.

There are several mechanisms presented in the literature for sub-surface initiated cracks. Voskamp [1] presents a mechanism based on tensile stresses that acts perpendicular to the contact surface of a ball in a raceway. The tensile stress appears during the unloading phase of an over-rolling sequence. Another mechanism that has been suggested for sub-surface fatigue is due to the shear stress amplitude, see for instance Fujii and Maeda [2]. Phenomena like inclusions and porosity may also be crucial to initiation of sub-surface cracks, see for instance Murakami and Endo [3].

The macro scale contacts in for example spur gears and roller bearings display contact situations with pressure distributions that more or less can be modelled as line contacts. Thus, it is of interest to investigate which type of contact fatigue cracks that can be produced by a two-dimensional line contact. For this reason a cylinder was repeatedly pressed against a plane test specimen. The test was named cylindrical standing contact fatigue. The idea was that this purified experiment would show that sub-surface contact fatigue can be produced by the two-dimensional macro scale contact, whereas surface initiated contact fatigue requires another explanation. Hence, the purpose was not to imitate applications of rolling contacts. The purpose was to find a mechanism for sub-surface contact fatigue. Dawson [4] performed similar contact fatigue tests with a cylindrical indenter without achieving sub-surface cracks.

Cylindrical Standing Contact Fatigue

For the experiments an SKF roller was used as indenter. Originally, the SKF roller ends contained a small crowning. Therefore the ends were cut off to obtain a purely cylindrical indenter. The specimens were taken from case-hardened circular steel plates with case material in the contact surface.

In order to minimize edge effects the width of the specimen was equal to that of the indenter. Thus, specimen and indenter were chosen pairwise, resulting in an average mismatch of 0.01 mm. See Fig. 1a for a view of the experimental set-up. To ensure that the indenter and specimen surfaces were parallel, an adjustable rig was used. The rig consisted of a plane that was balanced on an SKF bearing ball. The plane was fixed with four bolts when it was parallel to the indenter, see Fig. 1b.

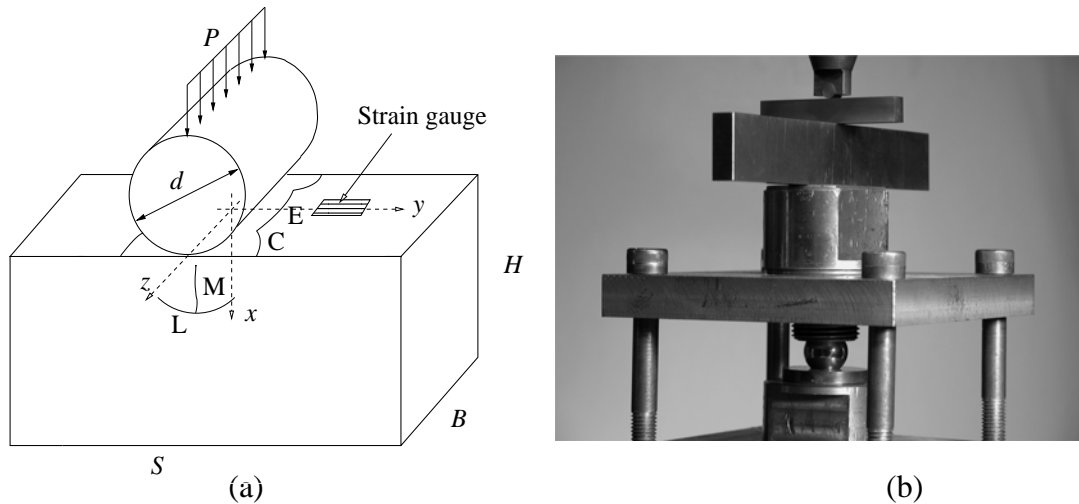


FIGURE 1. (a) Schematic of indenter and specimen, $S \times B \times H = 40 \times 6 \times 10$ mm, $d = 6$ mm. The four detected cracks are named as follows: L=Lateral crack, M=Median crack, C=Corner crack, E=Edge crack. (b) Test rig.

Contact fatigue experiments were performed with a pulsating load. The load was cycled from 0.2 kN to 12.2; 14.2; 16.2; 18.2; 20.2 kN. The minimum compressive load of 0.2 kN was set to avoid loss of contact between specimen and indenter during the tests. All tests were stopped at predefined number of cycles, which varied between 20 thousand and 2.5 million cycles. The advantage with this test method is that it has few adjustable parameters, which makes it easier to interpret the fatigue results. Parameters that can be alternated are load, geometry and material properties.

All test are performed without any lubrication. Crack initiation and propagation are therefore independent of mechanisms such as the “entrapped fluid mechanism”. Another parameter that is not involved in this test is the slip ratio, which is a frequently used parameter in rolling contact fatigue. It is however possible to include slip in this type of test by tilting the supporting plane. Furthermore, no damage at the surfaces has been detected in the current experiments that indicate the presence of fretting fatigue.

Material

The specimen material is Swedish standard SS2506. The material, is after case hardening, used in gears. In the x -direction, below the contact surface, the hardness varies from 800 HV to 400 HV, see Fig. 2a. In Fig. 2b the stress-strain relation for the case and core materials are shown. The core material displayed cyclic softening which is included in the curve for the core material. It was assumed that the result of the hardening process could be summarised in the free transformation strain that is included in Fig. 2a. The material property of an arbitrary point was combined from the case and core material properties using the transformation strain as a weight function, see Dahlberg and Alfredsson [5].

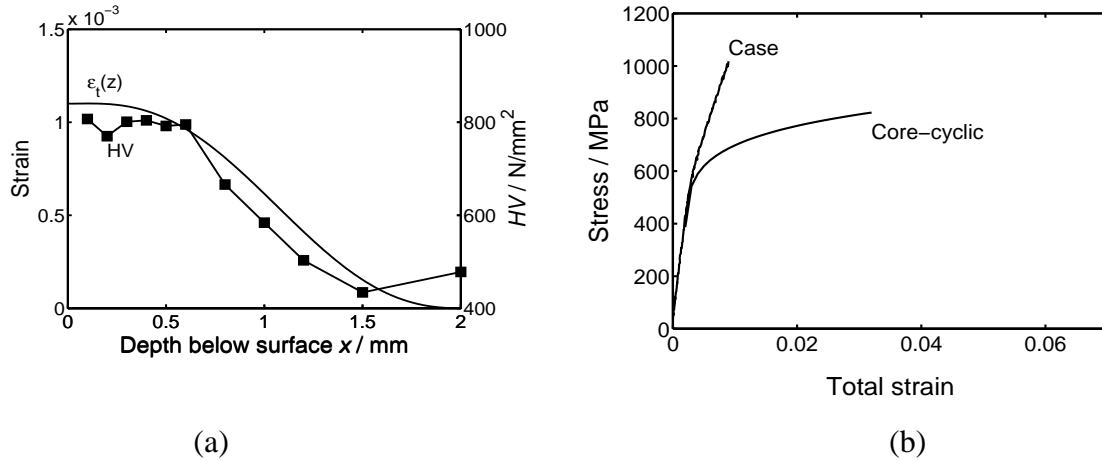


FIGURE 2. (a) Vickers hardness and transformation strain profiles below the contact surface. (b) Stress-strain relation for the case and core materials in the specimen.

Experimental results

In total, 38 test were performed. The fatigue limit turned out to be approximately 12.2 kN for the current arrangement. Focus was not to detect a lower fatigue limit, instead the crack initiations sites were of interest. In Figs 3 and 4a the resulting cracks are presented as they appear after finished tests. The presence of cracks of each type at test termination is compiled into Fig. 4b. By comparing crack types to number of load cycles and test load levels in Fig. 4b an order in which the cracks develop could be established.

Firstly the lateral crack initiates at the sides of the specimen, see Fig. 3a. With increasing load cycles the lateral cracks propagate out from the contact symmetry line and into the centre of specimen. As the crack grows into the specimen it also approaches the surface. Fig. 3b shows a lateral crack that has grown into the centre of the specimen.

The median cracks are vertically oriented and located between the lateral cracks and the contact surface. Also this crack type developed at the specimen sides, see Fig. 3a. These cracks only existed in combination with lateral cracks, which on the other hand may develop alone.

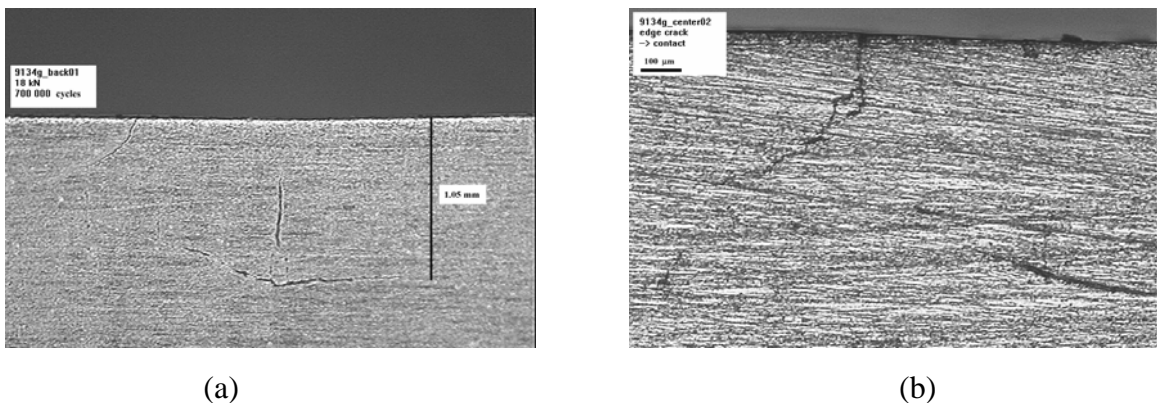


FIGURE 3. (a) Side view of specimen with lateral crack at 1.05 mm below the contact surface. Median and corner cracks are also visible. (b) The same specimen as in (a) but here a cut through the centre of the specimen is shown. The lateral and edge cracks are visible.

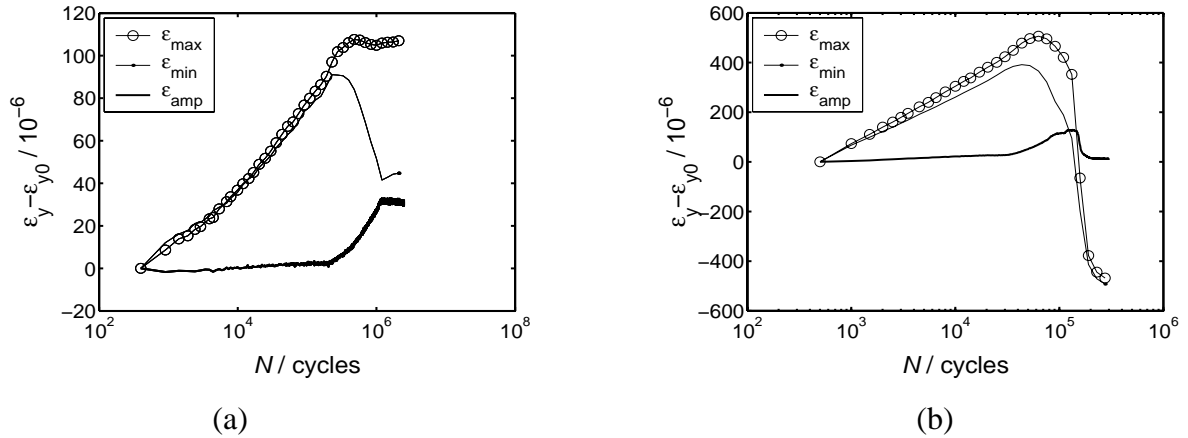


FIGURE 5. Strain response from two typical contact fatigue tests. (a) The load was 14.2 kN. Lateral and median cracks were present at test termination. (b) In this test the load was 18.2 kN and all four crack types were present after the experiment was stopped.

Numerical Computations

When the load was cycled the material reached an elastic steady state, after the initial phase with plastic deformation. In order to rapidly reach the elastic steady-state an isotropic hardening rule was used in the FE analysis. Both 2D- and 3D-models were used. The 2D-models were used to investigate how the different crack types affected the surface strain.

Fig. 6a presents the simulated surface strain response during load cycles before and after the lateral, median and edge cracks were introduced into the FE model. Two different plane strain 2D-models were used, one for the edge crack and one for the lateral and median cracks. Since the uncracked behaviour was equal in both models only the second, with lateral crack, was used to record the uncracked behaviour. Also due to the isotropic hardening rule, the models were elastic after the first peak load. Thus loading and unloading followed identical paths. The local plastic deformation at the crack tip did not affect the far field strain at the surface. The edge crack was opened at first peak load and gave a horizontal strain jump in Fig. 6a. The strain response with an edge crack was captured during the following unloading.

The lateral and median crack model was elastically unloaded from the first peak load to capture the elastic steady state strain response without any cracks. The lateral crack was then opened, which resulted in a horizontal strain jump at $P = 0$. The strain response with a lateral crack was recorded during the second load phase. The median crack was opened and the load was again removed to record the strain with both lateral and median cracks.

Thus, the influence of each crack type is documented in Fig. 6a. The lateral crack reduced ε_{min} and thus the increased ε_{amp} . The influence by the median crack was minimal. The edge crack, finally, reduced both ε_{min} and ε_{max} substantially.

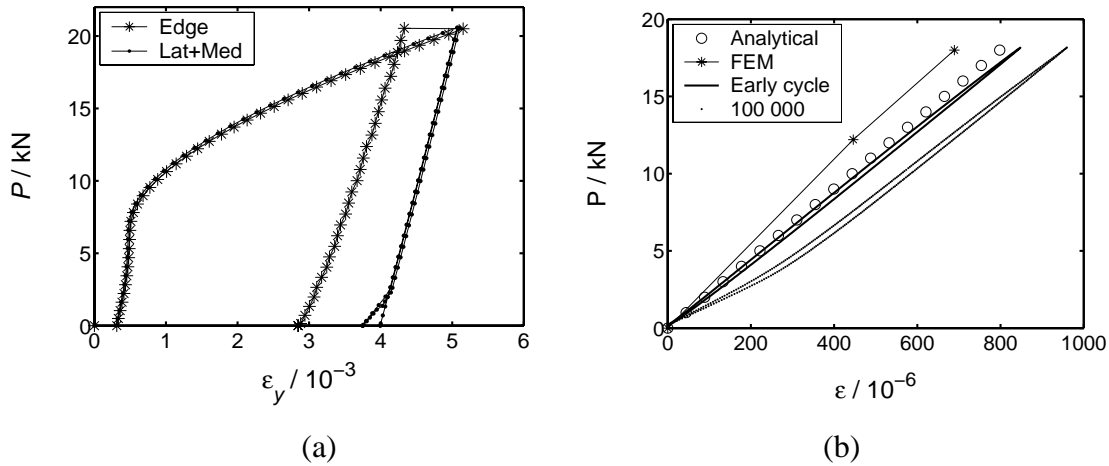


FIGURE 6. (a) Surface strain responses for different cracks in the 2D-model. The cracks were introduced at maximum load, or at $P = 0$, and resulted in strain jumps and changes in specimen compliance. (b) Measured surface strain at an early load cycle (solid line) and after 100 thousand cycles (curved line) compared to Eq.(1) and FE solution

The 3D-model was partly used to verify the 2D-models for plane stress and plane strain, partly to verify the non-zero surface strain response. The surface strain in the 3D- FE-model was integrated over the strain gauge position in the experiment that is illustrated in Fig. 6b. Also included in the figure is the prediction by Eq. (1) when integrated over the strain gauge position. The 3D-model contained 27624 elements. Stresses and plastic strains were investigated for coordinates where cracks had initiated. In Fig. 7a the residual stress σ_x is shown. The Findley fatigue criteria was computed and its local values are presented in Fig. 7b.

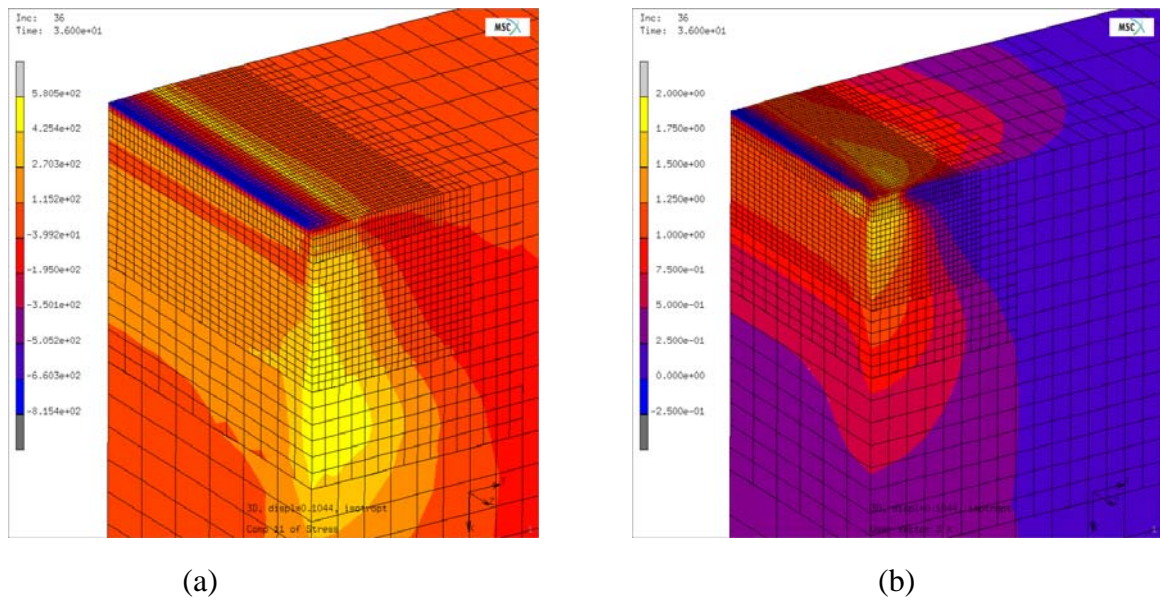


FIGURE 7. FEM results close to the contact for a load corresponding 18.2 kN. One quarter of the set-up in Fig. 1a was modelled. The indenter is not shown in the figures above. (a) The residual stress, σ_x . The maximum is found on the side of the specimen and is located at depth of 1.5 mm. (b) The maximum Findley value is located at a depth of 0.375 mm.

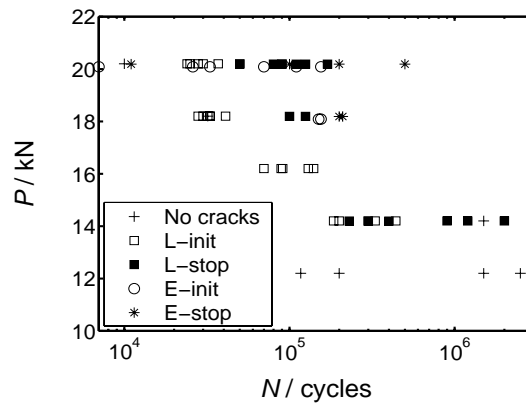


FIGURE 8. Number of load cycles to start and finish of the development of lateral and edge cracks captured by surface strain changes.

Discussion

The order in which the four crack types developed could be established by comparing the measured changes in surface strain response to the computed FE strain response. The FE predictions suggested that for the strain changes in Fig. 5a, the lateral crack developed between 0.2 million and 1.2 million cycles. For the experimental strain result in Fig. 5b, the lateral crack grew between 33 thousand and 100 thousand cycles, whereas the edge crack developed from the 150 thousand to the 200 thousand cycles.

The start and finish cycles for all cracks as indicated by the strain changes are compiled into Fig. 8. The predictions displayed a one to one correlation to actual crack presence at experimental ending as shown in Fig. 4b. Thus, in the standing contact fatigue experiments with a cylindrical indenter the sub-surface cracks appear before surface initiated cracks. Furthermore, the surface cracks require higher load levels to develop than the sub-surface cracks do. The implication for spalling or rolling contact fatigue was that the two-dimensional macro scale contact alone can produce sub-surface damage. These cracks are the result of tensile residual stress from unloading of a plastically deformed state. Thus, the mechanism suggested by Voskamp [1] for the initiation of sub-surface spalling in bearings was supported. The fact that surface cracks requires substantially increased load levels and number of load cycles to develop indicates that the two-dimensional contact can not alone produce surface spalling. The tensile surface stress from a finite specimen may however enhance the effects of another mechanism for surface initiated spalling.

Conclusions

Four types of contact fatigue cracks developed in cylindrical standing contact fatigue experiments. Two of these were of primary interest for spalling, namely the sub-surface lateral crack and the surface edge crack. These could be related to sub-surface and surface initiated spalling. It was concluded that a two-dimensional cyclic contact load may lead to sub-surface damage or spalling but highly unlikely to produce surface initiated spalling. For surface initiated spalling another mechanism is required.

The crack detection method with strain gauge on the contact surface was capable of detecting the beginning and the end of lateral and edge crack formation.

References

1. Voskamp, A.P., *ASTM Special Technical Publication*, v **1327**, 152-166, 1998.
2. Fujii, Y., Maeda, K., *Wear*, v**252**, 799-810, 2002.
3. Murakami, Y., Endo, M., *Journal of Basic Engineering*, v**16**, 163-182, 1994.
4. Dawson, H. P., *Journal Mechanical Engineering Science*, v **9(1)**, 67-80, 1967.
5. Dahlberg, J., Alfredsson, B., *Submitted for publication*.